

# Nanoscale

Accepted Manuscript



This is an *Accepted Manuscript*, which has been through the Royal Society of Chemistry peer review process and has been accepted for publication.

*Accepted Manuscripts* are published online shortly after acceptance, before technical editing, formatting and proof reading. Using this free service, authors can make their results available to the community, in citable form, before we publish the edited article. We will replace this *Accepted Manuscript* with the edited and formatted *Advance Article* as soon as it is available.

You can find more information about *Accepted Manuscripts* in the [Information for Authors](#).

Please note that technical editing may introduce minor changes to the text and/or graphics, which may alter content. The journal's standard [Terms & Conditions](#) and the [Ethical guidelines](#) still apply. In no event shall the Royal Society of Chemistry be held responsible for any errors or omissions in this *Accepted Manuscript* or any consequences arising from the use of any information it contains.

Cite this: DOI: 10.1039/c0xx00000x

www.rsc.org/xxxxxx

ARTICLE TYPE

# Controlled synthesis of highly dispersed BiPO<sub>4</sub> photocatalyst with surface oxygen vacancy

Zhen Wei,<sup>a</sup> Yanfang Liu,<sup>a</sup> Jun Wang,<sup>a</sup> Ruilong Zong,<sup>a</sup> Wenqing Yao,<sup>a</sup> Juan Wang<sup>b</sup> and Yongfa Zhu<sup>\*a</sup>

Received (in XXX, XXX) Xth XXXXXXXXX 20XX, Accepted Xth XXXXXXXXX 20XX

DOI: 10.1039/b000000x

Highly dispersed BiPO<sub>4</sub> with surface oxygen vacancy was synthesized via a solvothermal-calcination method. They can disperse uniformly in water for more than three days and the optimum photocatalytic activity of these highly dispersed BiPO<sub>4</sub> was more than twice as high as that of Degussa P25 due to the oxygen vacancy. The high dispersibility is attributed to a layer of organic matter formed on the surface of BiPO<sub>4</sub> via solvothermal approach. Most of the organic matter can be removed by calcination at 450°C, but a small amount of them remains, thus the calcinated BiPO<sub>4</sub> retained its high dispersibility. This high dispersibility maintains good contact between BiPO<sub>4</sub> and the pollutants, resulting in the efficient removal of the pollutants by BiPO<sub>4</sub>. Besides, calcination at 450°C also induced the formation of oxygen defects in BiPO<sub>4</sub>, which promotes the separation of photogenerated charge carriers and thus improving the photocatalytic activity of BiPO<sub>4</sub>.

## 1. Introduction

BiPO<sub>4</sub> was found to be a promising photocatalyst with better photocatalytic activity than Degussa P25 under UV light.<sup>1-4</sup> Furthermore, according to the previous report, it can be coupled with BiOI to obtain efficient visible light responsive photocatalyst with strong mineralization ability.<sup>5</sup> Zhu's group reported the core-shell structure of BiPO<sub>4</sub> with C<sub>3</sub>N<sub>4</sub> which showed dramatic photocatalytic activity under both visible light and UV light.<sup>6</sup> The photocatalytic activity of BiPO<sub>4</sub> can be improved greatly by introducing surface oxygen vacancy via hydrogen reduction<sup>7</sup>, vacuum deoxidation<sup>8</sup> and phase junctions.<sup>9</sup> Meanwhile, the efficiency of BiPO<sub>4</sub> for water splitting is also enhanced under UV light through coupling with reduced graphene oxide.<sup>10</sup>

Due to the tendency to agglutinate by Brownian Motion in solution, it is difficult to synthesize small and highly dispersed BiPO<sub>4</sub> nanoparticles. The low dispersibility of BiPO<sub>4</sub> has restricted its practical application seriously. Up to now, most of the reported methods can only be used to prepare BiPO<sub>4</sub> with the size larger than 100 nm. Though the minimum size of BiPO<sub>4</sub> was reported to be 9 nm,<sup>11</sup> these small nanoparticles could only be dispersed in non-polar solvent and the preparation conditions are complicated. Becerro et al. synthesized monodispersed BiPO<sub>4</sub> nanostars using a mixed solvent of glycerol and glycol, but the size of BiPO<sub>4</sub> was larger than 150 nm and the photocatalytic activity was low because of the existence of organics.<sup>12</sup> The usual way to synthesize aqueous dispersion nanoparticles is "Ligand-Exchange Method"-The nanocrystals in polar hydrophilic solvent to exchange the surface of hydrophobic molecules to improve its dispersibility in water.<sup>13-15</sup> But this method is complicated to operate and the conversion rate is low. Moreover, the hydrophilic organic molecules on the nanocrystal surface would drastically

reduce the separation efficiency of photogenerated carriers, and thus decrease the photocatalytic activity.<sup>16</sup> Therefore, it is necessary to find an efficient method to synthesize BiPO<sub>4</sub> particles with small size, high dispersibility and high photocatalytic activity.

Surface oxygen vacancy can prevent the electron-hole recombination to enhance the photocatalytic activity, such as TiO<sub>2</sub>,<sup>17, 18</sup> ZnO,<sup>19</sup> and Bi<sub>2</sub>WO<sub>6</sub>.<sup>20</sup> In this work, highly dispersed BiPO<sub>4</sub> nanoparticles was prepared by a solvothermal method with the size of 50-100 nm. The photocatalytic activity was greatly improved by the surface oxygen vacancy formed in the process of calcination. The influence of organic compounds on the morphology, dispersion, oxygen vacancy and photocatalytic activity of nanoparticles was investigated. Detailed mechanism for this influence was illustrated.

## 2. Experimental Section

### 2.1 Materials preparation

The highly dispersed BiPO<sub>4</sub> was synthesized via a solvothermal calcination route. All chemicals used were analytic grade reagents. In a typical procedure, 3 mmol of Bi(NO<sub>3</sub>)<sub>3</sub>·5H<sub>2</sub>O and Na<sub>3</sub>PO<sub>4</sub>·12H<sub>2</sub>O were dissolved in 15 mL ethylene glycol, respectively. Ethylene glycol solution of Na<sub>3</sub>PO<sub>4</sub> was slowly added drop wise to the Na<sub>3</sub>PO<sub>4</sub> solution with vigorously stirring, then was solvothermally treated at 25°C, 100°C, 120°C, 140°C, 160°C and 180°C for 48 h in a Teflon-lined autoclave of 40 mL capacity. The products were washed three times with ethanol and dried at 80°C for 12 h. The products were denoted as EG-25°C, EG-100°C, EG-120°C, EG-140°C, EG-160°C and EG-180°C, respectively. Take out part of these products and calcine them for 4 h at 450°C in air with the heating rate of 2°C/min, and the resulting products were denoted as cal.-25°C, cal.-100°C, cal.-

120°C, cal.-140°C, cal.-160°C and cal.-180°C, respectively. The time series products are synthesized as follows: Keep the solvothermal temperature at 140°C, change the reaction time from 0 to 96 h and other conditions are as described above.

For comparison, a control sample was synthesized according to reference [1] and it is denoted as SSR. 3 mmol  $\text{Bi}(\text{NO}_3)_3 \cdot 5\text{H}_2\text{O}$  and 3 mmol  $\text{Na}_3\text{PO}_4 \cdot 12\text{H}_2\text{O}$  were dissolved in 30 ml distilled water with vigorous stirring. Then transfer the precursor solution into a Teflon-lined stainless steel autoclave which was maintained at 180°C for 72 h to synthesize the products. The as-prepared products were washed with distilled water several times and dried for 12 h. The SSR calined at 450°C for 4h was donated as c-SSR.

## 2.2 Characterization of products

In order to investigate the phase structure, the products were characterized by X-ray diffraction (XRD, Bruker D8-advance X-ray diffractometer) with  $\text{Cu K}\alpha 1$  ( $\lambda = 1.5418 \text{ \AA}$ ) radiation at 40 kV and 40 mA. In order to investigate the morphologies, the samples were characterized by transmission electron microscopy (TEM, Hitachi 7700) with a voltage of 100 kV and high-resolution transmission electron microscope (HR-TEM, JEM2010E) with an accelerating voltage of 200 kV. In situ electron paramagnetic resonance (EPR) measurement was taken in an Endor spectrometer (JEOL ES-ED3X) at 103 K in liquid nitrogen. The g factor was obtained by taking the signal of manganese as standard. Magnetic parameters of radicals were obtained by direct measurements of the magnetic field and microwave frequency. To characterize the chemical composition, samples were recorded by X-ray photoelectron spectroscopy (ESCALAB 250Xi, ThermoScientific) with charging effect calibrated by binding energy of C1s orbital. Elemental analysis results were collected from an EA3000 analyzer. FTIR spectra (Bruker V70FTIR) were measured from 4000  $\text{cm}^{-1}$  to 600  $\text{cm}^{-1}$ . Raman spectra were conducted by using a HORIBA JYHR800 confocal microscope Raman spectrometer employing an Ar<sup>+</sup> laser (514.5 nm). Thermogravimetric analysis was measured by Mettler TGA/DSC 11600 under O<sub>2</sub> atmosphere with a heating rate of 10 °C/min. Zeta potential was taken on HORIBA SZ-100 series analyzer.

## 2.3 Evaluation of catalytic activity

The photocatalytic activity of the products was evaluated by their efficiency for degrading MB solution under the irradiation of UV light, which was provided by a mercury lamp (Institute for Electric Light Sources, Beijing) at 20 W. The average light intensity was 0.70  $\text{mW}/\text{cm}^2$  and the wavelength of UV light is 254 nm. The as-prepared photocatalysts were added into 50 mL MB solution with concentration of  $2 \times 10^{-5}$  M and ultrasonically dispersed for 30 min in the dark. The solution was stirred for 30 min in the dark before irradiation to reach the absorption-desorption equilibrium. 3 mL solution was sampled and centrifuged to remove the photocatalyst. The MB supernatant was analyzed by UV-vis spectrophotometer. The degradation processes of  $2 \times 10^{-5}$  M RhB solution,  $2 \times 10^{-5}$  M MO solution and 25 ppm phenol solution were similar to that of MB.

The photoelectrochemical measurements were carried out in a conventional three-electrode system with ITO/ $\text{BiPO}_4$  electrode as the working electrode, a platinum wire as the counter electrode and a standard calomel electrode as the reference electrode. 0.1 M

$\text{Na}_2\text{SO}_4$  solution was used as the electrolyte solution. The photoelectric response was measured at 0.0 V. 5 mg photocatalyst was suspended in 1 mL ethanol and then was dip-coated on a 2×4 cm ITO glass to make the working electrode. The as-prepared electrode was then dried at 80 °C for 12 h in the air.

## 3. Results and discussion

### 3.1 High-dispersion and dispersion mechanism

In order to investigate the dispersion capability of the prepared samples, SSR, EG-140°C and cal.-140°C were dispersed into water to form 0.1% (mass percent) suspensions without any dispersants or additives. The photographs of the suspensions after still standing for different time period are shown in Fig.1A. The SSR sample subsided obviously after 2 hours and after 24 hours it subsided to the bottom completely, while EG-140°C and cal.-140°C suspensions did not change much and only about 1/4 of the suspensions subsided after 72 hours' still standing. The dispersion experiment shows that EG-140°C and cal.-140°C have good dispersion performance which may be attributed to the organics on the surface of  $\text{BiPO}_4$ .

Zeta potentials of the solutions were shown in Fig.1B. The larger the absolute value of Zeta potential is, the more stable the solution is. When the absolute value of Zeta potential is larger than 30 mV, the particles are dispersed well in the solution. EG-140°C, cal.-140°C, and SSR are all electronegative. The Zeta potentials of EG-140°C, cal.-140°C, and SSR are -46.4 mV, -45.8 mV, and -5.0 mV respectively. The absolute values of EG-140°C and cal.-140°C solution are larger than 30 mV, while that of SSR is far smaller than 30 mV. This means that EG-140°C and cal.-140°C can disperse stably in water while SSR cannot, which corresponds to the sedimentation experiment.

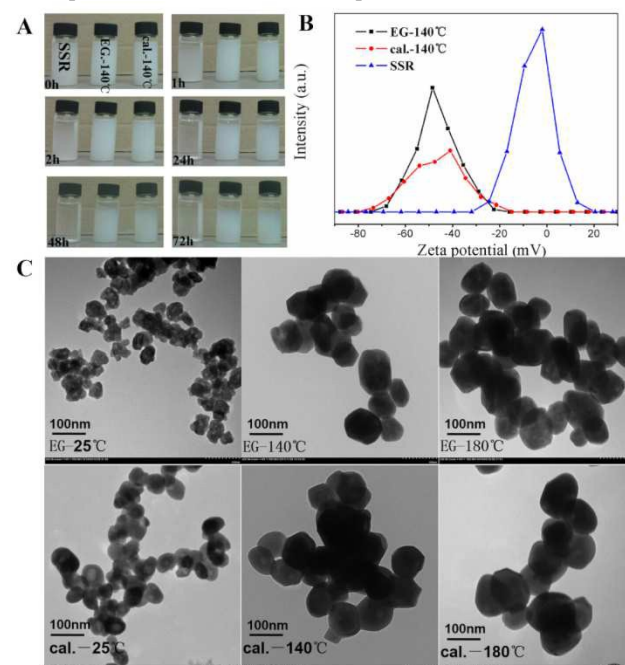


Fig. 1 Photographs of 0.1w% SSR, EG-140°C, and cal.-140°C solutions after standing for different times (A). Zeta potentials of 0.1 w% SSR, EG-140°C, and cal.-140°C solutions (B). TEM images of samples prepared at different temperatures for 48 h (upper images in C). The corresponding images of samples after calcination at 450°C for 4 h (lower images in C)

Based on the XRD results (Fig.S1A), all the samples were monazite monoclinic structure (JCPDS No.89-0287, space group: P21/n), indicating that the solvothermal and calcination processes did not change the crystal phase of BiPO<sub>4</sub>. The TEM images of the samples treated with different solvothermal time and temperature and their calcination samples are shown in Fig. 1C, S1B, S1C and S1D. The morphologies of the samples treated with the solvothermal temperature below 140°C are not uniform and their crystallinity is low. When the solvothermal temperatures were in the range of 140°C~180°C, with the increase of temperature, the particle morphologies became more uniform, indicating that the crystallinity was becoming better. As is shown in Fig. S1B, the relationship between the reaction time and morphology is the same as that between solvothermal temperature and morphology. When the reaction time was longer than 48 h, the samples become uniform particles with diameters

of about 50~100 nm. After calcination at 450°C for 4 h, the samples prepared below 140°C grew further to form uniform particles, while the samples prepared above 140°C maintained their polyhedron morphologies.

The formation mechanism of the polyhedral morphology is closely related to the nature of the solvent. Ethylene glycol coordinates with Bi<sup>3+</sup> to form alkoxides, which decreases the concentration of Bi<sup>3+</sup> and further decreases the nucleation rate of BiPO<sub>4</sub>. The nanocrystals formed in ethylene glycol solution have fewer surface hydroxyl groups and suffers from larger viscosity compared with that in water, making the nanocrystals turnover much slower. This slow turnover rate of nanocrystals renders them in uniform polyhedral morphology to obtain the lowest energy configuration.<sup>16, 21</sup> The small particle size of these polyhedral products also improves the dispersion capability due to their small gravity.

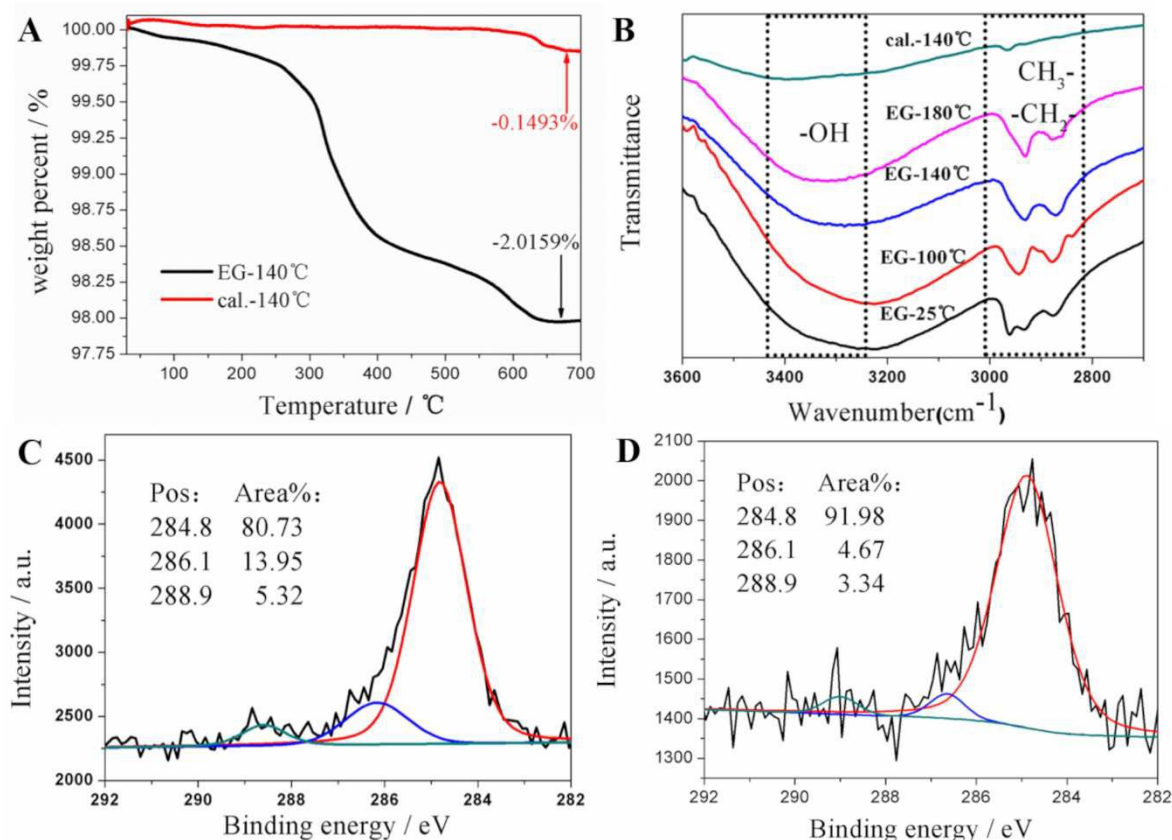


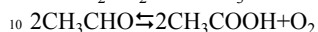
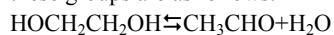
Fig. 2(A) The TGA curve of EG-140°C and cal.-140°C. (B) The FTIR spectra (3600-2700 cm<sup>-1</sup>) of samples prepared by different solvothermal temperatures and samples after calcination. (C) The high-resolution XPS spectrum of C1s in EG-140°C. (D) The high-resolution XPS spectrum of C1s in cal.-140°C.

The photocatalytic activity and dispersion capability are related to the amount and kinds of organic group species on the surface of the photocatalysts. The TGA of sample EG-140°C and cal.-140°C under oxygen atmosphere is shown in Fig. 2A. EG-140°C has an obvious weight loss under 400°C while cal.-140°C only has a little change at 600°C. The weight loss of EG-140°C and cal.-140°C are 2.0159% and 0.1493% (Table 1) respectively in the whole process. This result shows that EG-140°C contains more organics than cal.-140°C. In order to determine the types of organics on the surface, FTIR measurement (Fig. 2B) was conducted. Sample EG-25°C, EG-100°C, EG-140°C, and EG-

180°C all have strong peaks at 2960 cm<sup>-1</sup>, 2870 cm<sup>-1</sup>, 2930 cm<sup>-1</sup>, and 2850 cm<sup>-1</sup> corresponding to the absorption of methyl and methylene group. The FTIR peak intensities of cal.-140°C are much weaker than those of the samples without calcination, revealing that most of the surface organics can be removed by calcination.<sup>22</sup> The peak at 3300 cm<sup>-1</sup> corresponds to the stretching vibration of hydroxyl group. The intensity of this peak is weaker in cal.-140°C compared with that in EG-140°C because the organics containing hydroxyl group is removed by calcination.<sup>23</sup>

In order to investigate the elemental composition of the organics, X-ray photoelectron spectra measurements of EG-

140°C and cal.-140°C (Fig. 2C and 2D) were examined. The XPS spectra of C 1s for EG-140°C and cal.-140°C can be divided into three peaks. The strongest peak at 284.8 eV is ascribed to contaminant C. The two peaks at 286.1 eV and 288.9 eV are attributed to C=O, C-O, COR(H) groups on the surface of BiPO<sub>4</sub>.<sup>23, 24</sup> These groups come from ethylene glycol during the preparation process of BiPO<sub>4</sub>.<sup>22, 25</sup> The formation mechanisms of these groups are as follows:



The oxygen atoms in these aldehydes, acids, and alcohols can form hydrogen bond with hydroxyl groups on BiPO<sub>4</sub> and change the surface properties of BiPO<sub>4</sub>. Based on the XPS results, the overall carbon content on the surface of EG-140°C and cal.-140°C are 35.50% and 15.91% respectively. Subtracting the polluted carbon, the surface organic carbon content are 6.84% and 1.27% respectively. There is a significant decrease of carbon content after calcination which shows calcination can remove

some of the organic carbon.

Table 1. Carbon content analysis of EG-140°C and cal.-140°C.

Sample	Carbon content (XPS)	Weight loss of TGA	Carbon content (Elemental analysis)
EG-140°C	6.84%	2.02%	0.83%
cal.-140°C	1.27%	0.15%	0.4%

In order to analyze the content of organic carbon in the whole particle, the elemental analysis measurement was performed. It can be seen from Table. 1 that the carbon content of EG-140°C and cal.-140°C are 0.83% and 0.4%, respectively. This result shows the organic materials were reduced a lot after calcination of BiPO<sub>4</sub>. Organic materials on the surface of catalyst may improve the dispersion ability while appropriate reduction of the organics can increase the activity amazingly.

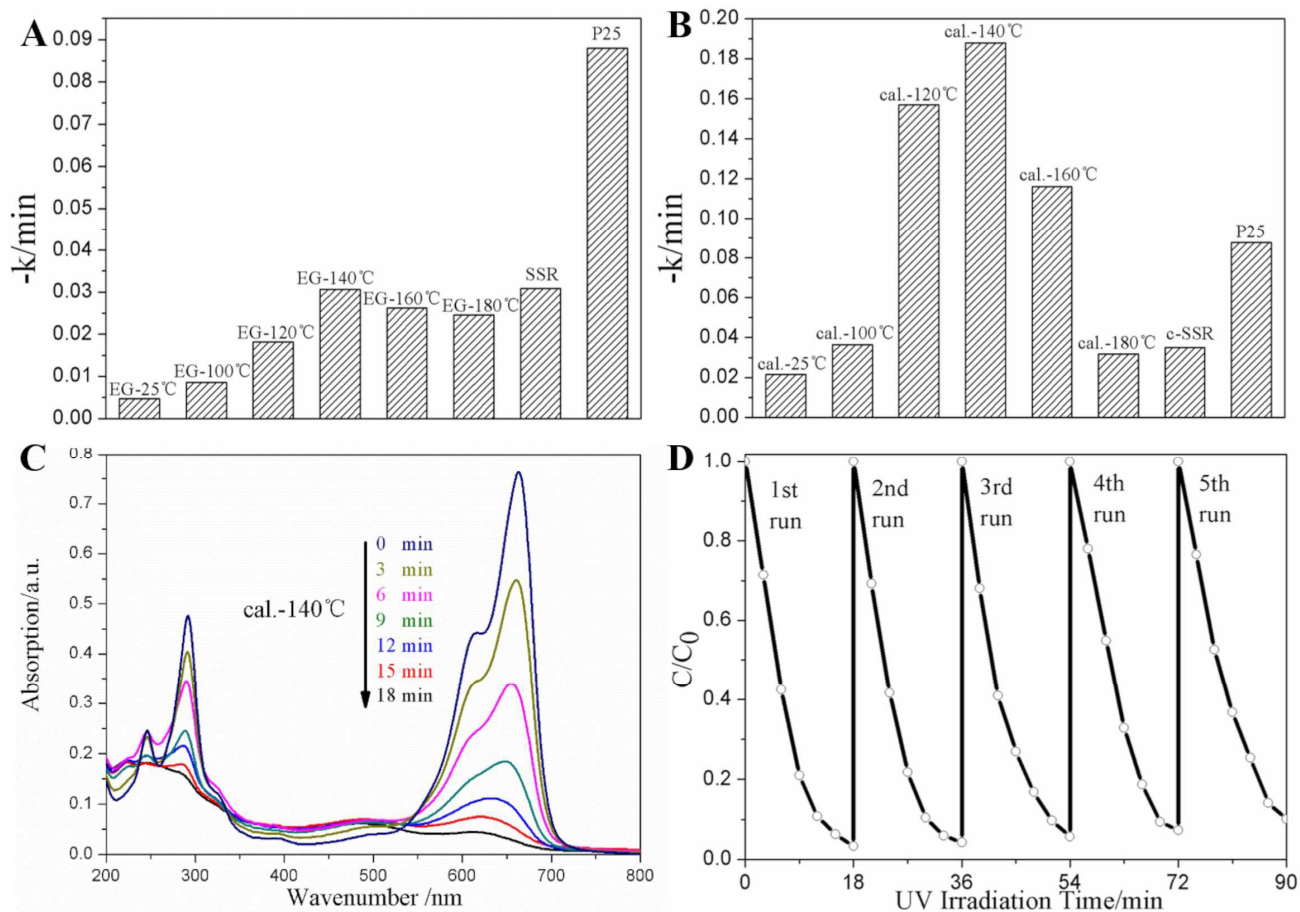


Fig. 3 (A) Degradation activities of samples synthesized at different temperatures (MB solution  $2 \times 10^{-5}$  mol/L); (B) Activities of samples synthesized at different solvothermal temperatures with calcination (MB solution  $2 \times 10^{-5}$  mol/L). (C) UV-vis spectra of MB solution degraded by cal.-140°C after 27 minutes (MB solution  $2 \times 10^{-5}$  mol/L). (D) UV photocatalytic degradation of MB ( $2 \times 10^{-5}$  mol/L) by cal.-140°C for five times.

### 3.2 High-activity and degradation mechanism

The photocatalytic activity were evaluated by degrading methylene blue (MB) solution, with commercial Degussa P25 being the control sample. The degradation process of MB solution followed quasi first order kinetic equation; the apparent rate constant  $k$  can be obtained by fitting the first order equation and it can be used to evaluate the photocatalytic activity of the samples. The apparent rate constant  $k$  of the samples synthesized

under different solvothermal temperatures for 48 h and after calcination at 450°C are shown in Fig. 3A and 3B respectively. With the increase of solvothermal temperature, the activity of the synthesized samples first increased and then decreased both before and after calcination. Before calcination (Fig. 3A), the activity of BiPO<sub>4</sub> synthesized at 140°C is the best. When the solvothermal temperature is lower than 140°C, the crystallinity of the synthesized BiPO<sub>4</sub> improves with the

solvothermal temperature (Fig. S1C). Lots of defects in the poorly crystallized samples could act as an electron-hole recombination center, resulting in the low photocatalytic activity.<sup>26</sup> When the solvothermal temperature is higher than 140 °C, the crystallinity of the samples are improved, but there are larger amount of organics on these samples, which decreases the photocatalytic activity. Therefore, both EG-120°C and EG-160°C display lower photoactivity than EG-140°C. But the activity of EG-140°C is still lower than that of P25. However, after calcination (Fig. 3B), the activities of all samples are increased compared with the uncalcinated ones. The samples synthesized at 120°C, 140°C, and 160°C all possess better photocatalytic activity than P25. Among them, the sample synthesized at 140°C and calcined at 450°C possesses the optimum photocatalytic activity, which is more than twofold higher than that of P25. Fig.

3C is the UV-vis absorption spectrum of MB solution degraded by cal.-140°C. MB solution could be completely degraded by cal.-140°C in about 15 minutes. With the increase of irradiation time, the intensity of absorption peaks of MB at 245 nm, 291 nm, and 663 nm decreased dramatically. There was no characteristic absorption peak of LMB at 256 nm, which shows the mechanism of degradation is direct oxidation, not through the reduction route to LMB.<sup>27</sup> The decrease of the absorption intensity at 290 nm shows that benzene ring was cracked down in the degradation process. The apparent rate constant  $k$  for the degradation of MB solution by BiPO<sub>4</sub> synthesized by different solvothermal times is shown in Fig. S4A. As shown in Fig. S4A, the photocatalytic activity of the synthesized BiPO<sub>4</sub> increases with the increase of solvothermal time when the latter is shorter than 48 hours and then keeps constant between 48 h and 96 h.

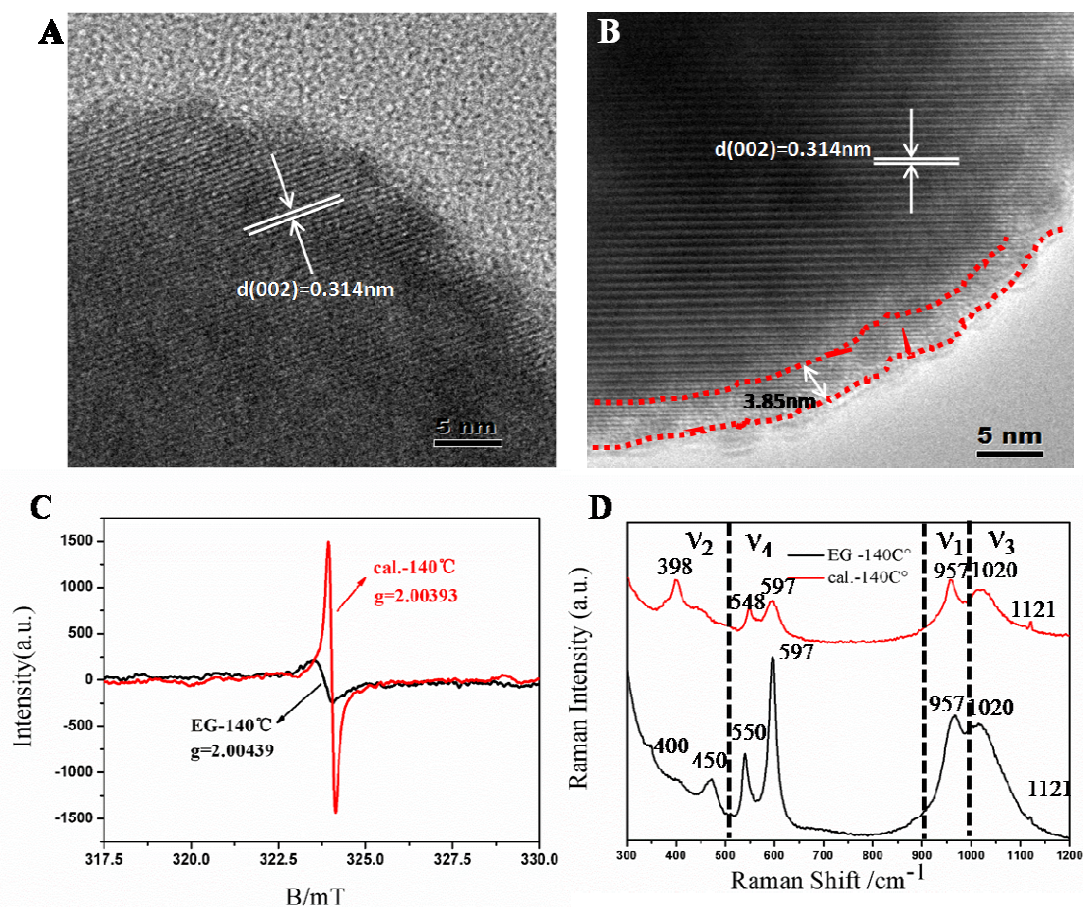


Fig. 4 HRTEM image of EG-140°C (A) and cal.-140°C (B); (C) Situ EPR spectra of EG-140°C and cal.-140°C at 103 K. (D) Raman spectrum of EG-140°C and cal.-140°C.

The degradation experiments of anionic dye (Methyl orange), cationic dye (Rhodamine B) and colorless organic pollutant (Phenol) by cal.-140°C and SSR samples were conducted to evaluate the selectivity of cal.-140°C. The apparent rate constant  $k$  is shown in Fig. S4B. The photocatalytic activity of cal.-140°C is 3 to 4 times as high as that of SSR no matter what kind of pollutant the degrading substrate is. This result shows the high activity of cal.-140°C is not caused by the specific absorption of certain pollutant but by the intrinsic nature of the material. Based on the liquid chromatography results (Fig. S4C and Fig. S4D), it only needs 60 minutes to degrade 25 ppm phenol completely, while the removal rate of phenol by the control sample is rather

low after 60 minutes. Interestingly, we find that the degradation rate of RhB is larger than that of MO under the same condition which may be induced by the negative charge on the surface of cal.-140°C, consistent with the Zeta potential data.<sup>11</sup>

In order to evaluate the stability of the photocatalyst, cyclic degradation experiments were conducted. Fig 4D and S5 show that there is hardly any obvious loss of activity after 5 cycles. The XRD patterns of BiPO<sub>4</sub> before and after degradation experiment show that though there is a little decrease of absolute peak intensity, the relative peak intensity remains the same which is consistent with JCPDS 89-0287. The crystal structure does not change during the experiment. In order to illustrate the storage

stability of the catalyst, cal.-140°C stored for 15 months and the fresh cal.-140°C were made a comparison (Fig. S6). The photocatalytic activity of cal.-140°C after storage for 15 months only decreases slightly ( $k = 0.186 \text{ min}^{-1}$ ), compared with that of fresh cal.-140°C ( $k = 0.188 \text{ min}^{-1}$ ). These two tests indicate that cal.-140°C has a good stability on both photocatalytic degradation and storage.

### 3.3 Formation of Surface Oxygen Vacancy

In order to explain why the calcined samples have so high photocatalytic activity, HRTEM measurement was conducted to examine the detailed structure of the samples before and after

calcination (Fig. 4A and Fig. 4B). From the HRTEM results, the clear lattice fringe images of EG-140°C and cal.-140°C samples indicate the good crystalline of both samples and the lattice spacing is about 0.314 nm corresponding to the (002) plane. The edge of lattice fringe in cal.-140°C becomes blurred, indicating the destruction of surface structure and the formation of defect structure in this sample.<sup>7, 8</sup> It is well known that a certain concentration of surface defect may improve the activity of photocatalysts.<sup>20</sup> The brilliant photocatalytic activity comes from its surface defect, which increase the separation speed of photo-generated carriers.

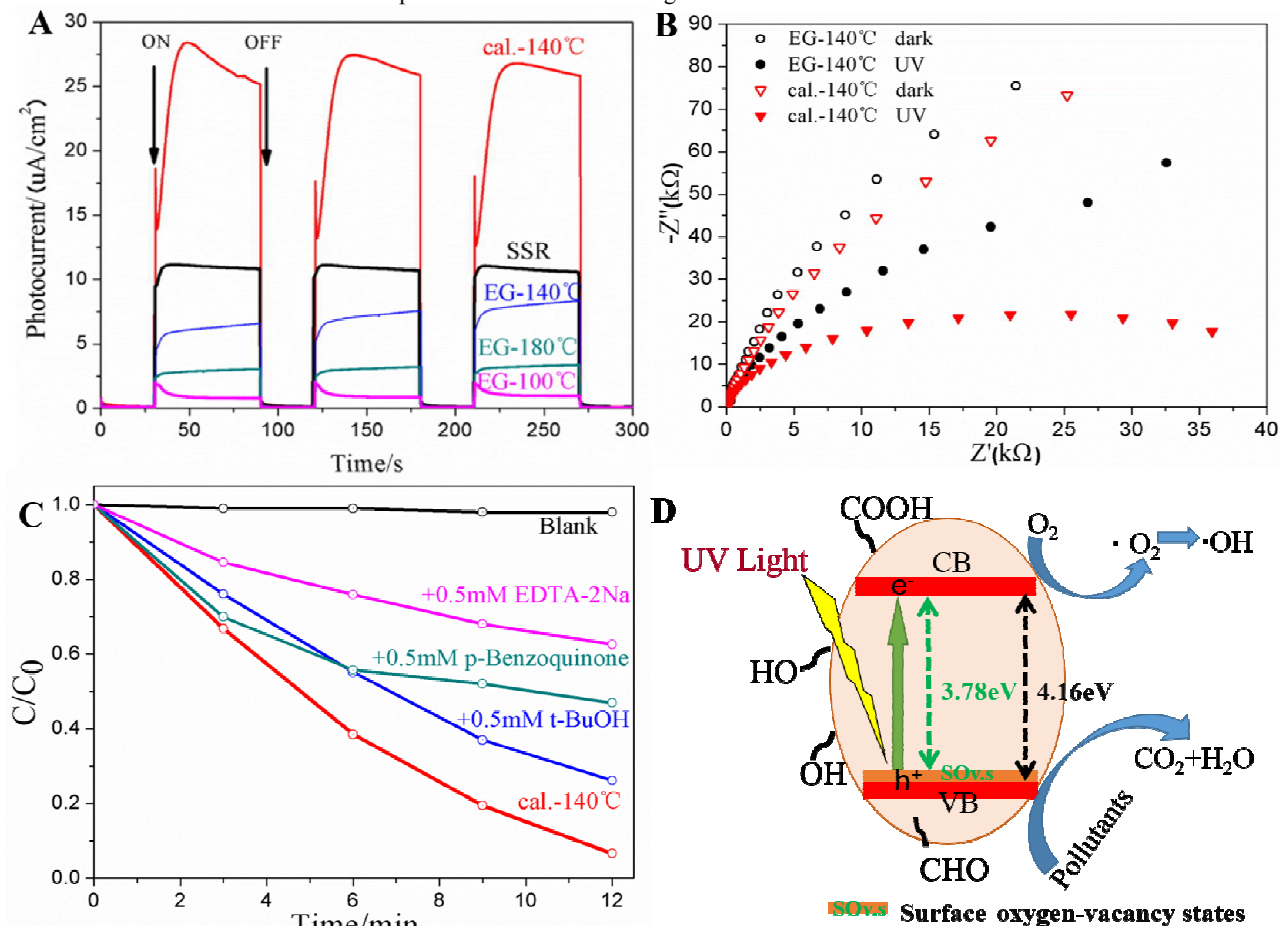


Fig. 5 (A) Photocurrents of samples after deposition on ITO electrodes, under UV light ( $\lambda = 254 \text{ nm}$ ); (B) Electrochemical impedance spectroscopy of EG-140°C and cal.-140°C; (C) The diagram of photogenerated carriers trapping in degradation of MB by cal.-140°C; (D) Mechanism of photocatalytic activity of cal.-140°C.

To further confirm the existence and properties of the surface oxygen vacancy, in situ electron paramagnetic resonance (EPR) was performed at 103 K in liquid  $\text{N}_2$ , which is a sensitive and direct method to monitor various behaviors of the oxygen defects.<sup>26</sup> The intensity of the EPR signal at  $g \sim 2.003$  of cal.-140°C is much higher than that of EG-140°C under the same conditions, as seen from Fig. 4C (the value of  $g$  was calculated by  $g = \text{hn/mBhr}$ ). As reported previously,  $g$  equal to  $2.003 \pm 0.001$  can be attributed to oxygen vacancies on the surface,<sup>29, 30</sup> indicating that surface oxygen vacancies were produced on calcined EG-140°C.

The structure of EG-140°C and cal.-140°C samples were also further characterized by Raman spectroscopy (Fig. 4D). The Raman peaks at  $1020 \text{ cm}^{-1}$  and  $957 \text{ cm}^{-1}$  correspond to  $\nu_3(\text{PO}_4)$

asymmetry stretching and the  $\nu_1(\text{PO}_4)$  symmetry stretching, respectively. The Raman spectrum bands at  $597 \text{ cm}^{-1}$  and  $550 \text{ cm}^{-1}$  correspond to  $\nu_4(\text{PO}_4)$  bending vibration, while cal.-140°C shift to  $548 \text{ cm}^{-1}$  and the peak intensity of EG-140°C at  $597 \text{ cm}^{-1}$  and  $548 \text{ cm}^{-1}$  are larger than those of cal.-140°C, which could be attributed to the contribution of oxygen vacancies. The Raman shifts at  $471$ ,  $398$  and  $349 \text{ cm}^{-1}$  are considered to result from the  $\nu_2$  bending modes of the  $\text{PO}_4$  units.<sup>31, 32</sup> The Raman spectra of  $\text{BiPO}_4$  after calcination is similar to that of  $\text{BiPO}_4$  prepared through  $\text{H}_2$  reduction method by Lv et al.,<sup>7</sup> indicating that the samples after calcination has surface oxygen vacancy.

### 3.4 Mechanism of the enhanced photocatalytic activity

The migration ability and separation efficiency of photo-generated charges have an important influence on the activity.

Fig. 5A is the photocurrents of samples. It can be seen that cal.-140°C has the highest photocurrent response which is twice as high as that of SSR and three times as high as the samples without calcination. Such a high photocurrent means a much quicker migration rate and a higher separation efficiency of photo-generated carriers in cal.-140°C. The quick migration rate and high separation efficiency of photo-generated carriers are the main reason for the high efficiency of cal.-140°C, which is in accordance with the degradation experiments. Fig. 5B is the electrochemical impedance spectroscopy (EIS) Nyquist plots of the samples. The smaller the arc radius of the EIS Nyquist plot, the higher the efficiency of charge separation. The radius on the EIS Nyquist plot of cal.-140°C is smaller than that of EG-140°C, indicating that calcinations of the samples could enhance the separation efficiency of charge carriers and thus enhanced their photocatalytic activity. This enhanced separation efficiency of charge carriers may be caused by the removal of surface organics and the formation of surface oxygen vacancy.

The photocatalytic mechanism can be traced by trapping experiments. Fig. 5C is the degradation curves of trapping experiment. We add scavengers in the MB solution, with EDTA-2Na as the hole scavenger,<sup>8</sup> p-Benzoquinone as the superoxide radical scavenger<sup>33</sup> and tertiary butanol as the •OH scavenger.<sup>34</sup> The concentration of these three trapping agents are all 0.5 mM. It can be seen from Fig. 6C that the addition of trapping agents can decrease the degradation rate of MB solution. EDTA-2Na decreased the rate most significantly, indicating the holes are the major oxidative species. The band gap of pure monoclinic BiPO<sub>4</sub> and BiPO<sub>4</sub> with surface oxygen vacancy (cal-140°C) are about 4.16 and 3.78 eV, respectively (Fig. S8).<sup>7, 8</sup> Based on the above analysis, the mechanism for the high dispersion capacity and excellent photocatalytic activity of the products prepared by solvothermal-calcination method are illustrated in Fig. 5D.

#### 4. Conclusions

The surface oxygen vacancy of BiPO<sub>4</sub> photocatalyst with high activity, high dispersion capacity and high stability was synthesized by a solvothermal-calcination method. The BiPO<sub>4</sub> synthesized in glycol solution has a hydrophilic organic structure on the surface, leading to its high dispersion capacity. Most of the surface organics are removed after calcination, inducing the formation of surface oxygen vacancy. The surface oxygen vacancy increases the migration ability of photo-generated charges and separation ability of photo-generated carriers, which increase the photocatalytic activity. Meanwhile, the thin layer of the remnant organics helps BiPO<sub>4</sub> retain its high dispersion capacity.

#### Acknowledgments

This work was partly supported by National Basic Research Program of China (973 Program) (2013CB632403), National High Technology Research and Development Program of China (2012AA062701) and Chinese National Science Foundation (21437003, and 21373121).

#### Notes and references

- <sup>a</sup>Department of Chemistry, Beijing Key Laboratory for Analytical Methods and Instrumentation, Tsinghua University, Beijing, 100084, China. E-mail: zhuyf@tsinghua.edu.cn
- <sup>b</sup>College of Chemistry and Chemical Engineering, Hubei University, Wuhan 430062, China
- † Electronic Supplementary Information (ESI) available: [details of any supplementary information available should be included here]. See DOI: 10.1039/b000000x/
- ‡ Footnotes should appear here. These might include comments relevant to but not central to the matter under discussion, limited experimental and spectral data, and crystallographic data.
- C. Pan and Y. Zhu, *Environ. Sci. Technol.*, 2010, **44**, 5570-5574.
  - Y. Liu, Y. Zhu, J. Xu, X. Bai, R. Zong and Y. Zhu, *Appl. Catal., B*, 2013, **142**, 561-567.
  - Y. Zhang, R. Selvaraj, M. Sillanpää, Y. Kim and C.-W. Tai, *Chem. Eng. J.*, 2014, **245**, 117-123.
  - C. Pan and Y. Zhu, *Catal. Sci. Technol.*, 2015, **5**, 3071-3083.
  - Y. Liu, W. Yao, D. Liu, R. Zong, M. Zhang, X. Ma and Y. Zhu, *Appl. Catal., B*, 2015, **163**, 547-553.
  - C. Pan, J. Xu, Y. Wang, D. Li and Y. Zhu, *Adv. Funct. Mater.*, 2012, **22**, 1518-1524.
  - Y. Lv, Y. Liu, Y. Zhu and Y. Zhu, *J. Mater. Chem. A*, 2014, **2**, 1174-1182.
  - Y. Lv, Y. Zhu and Y. Zhu, *J. Phys. Chem. C*, 2013, **117**, 18520-18528.
  - Y. Zhu, Y. Liu, Y. Lv, Q. Ling, D. Liu and Y. Zhu, *J. Mater. Chem. A*, 2014, **2**, 13041-13048.
  - B. Pan, Y. Wang, Y. Liang, S. Luo, W. Su and X. Wang, *Int. J. Hydrogen Energy*, 2014, **39**, 13527-13533.
  - C. Pan and Y. Zhu, *J. Mater. Chem.*, 2011, **21**, 4235-4241.
  - A. I. Becerro, J. Criado, L. C. Gontard, S. Obregón, A. Fernández, G. Colón and M. Ocaña, *Cryst. Growth Des.*, 2014, **14**, 3319-3326.
  - T. Zhang, J. Ge, Y. Hu and Y. Yin, *Nano Lett.*, 2007, **7**, 3203-3207.
  - A. Dong, X. Ye, J. Chen, Y. Kang, T. Gordon, J. M. Kikkawa and C. B. Murray, *J. Am. Chem. Soc.*, 2010, **133**, 998-1006.
  - D. Ling, M. J. Hackett and T. Hyeon, *Nano Today*, 2014, **9**, 457-477.
  - L. Jing, W. Zhou, G. Tian and H. Fu, *Chem. Soc. Rev.*, 2013, **42**, 9509-9549.
  - M. Kong, Y. Li, X. Chen, T. Tian, P. Fang, F. Zheng and X. Zhao, *J. Am. Chem. Soc.*, 2011, **133**, 16414-16417.
  - X. Pan, M.-Q. Yang, X. Fu, N. Zhang and Y.-J. Xu, *Nanoscale*, 2013, **5**, 3601-3614.
  - Y. Lv, C. Pan, X. Ma, R. Zong, X. Bai and Y. Zhu, *Appl. Catal., B*, 2013, **138**, 26-32.
  - J. Tian, Y. Sang, G. Yu, H. Jiang, X. Mu and H. Liu, *Adv. Mater.*, 2013, **25**, 5075-5080.
  - X. Zhang, Z. Ai, F. Jia and L. Zhang, *J. Phys. Chem. C*, 2008, **112**, 747-753.
  - G.-B. Shan and G. P. Demopoulos, *Nanotechnology*, 2010, **21**, 025604.
  - Y.-H. Tseng and C.-H. Kuo, *Catal. Today*, 2011, **174**, 114-120.
  - P. Ząbek, J. Eberl and H. Kisch, *Photoch. Photobio. Sci.*, 2009, **8**, 264-269.
  - M. Janus, B. Tryba, M. Inagaki and A. Morawski, *Appl. Catal., B*, 2004, **52**, 61-67.
  - C. Zhang and Y. Zhu, *Chem. Mater.*, 2005, **17**, 3537-3545.
  - H. Park and W. Choi, *J. Phys. Chem. B*, 2005, **109**, 11667-11674.
  - M. Y. Guo, A. M. C. Ng, F. Liu, A. B. Djuricic, W. K. Chan, H. Su and K. S. Wong, *J. Phys. Chem. C*, 2011, **115**, 11095-11101.
  - C. F. Windisch Jr, G. J. Exarhos, C. Yao and L.-Q. Wang, *J. Appl. Phys.*, 2007, **101**, 123711.
  - Y. Li, D.-S. Hwang, N. H. Lee and S.-J. Kim, *Chem. Phys. Lett.*, 2005, **404**, 25-29.
  - J. Geng, W.-H. Hou, Y.-N. Lv, J.-J. Zhu and H.-Y. Chen, *Inorg. Chem.*, 2005, **44**, 8503-8509.
  - G. Li, Y. Ding, Y. Zhang, Z. Lu, H. Sun and R. Chen, *J. Colloid Interf. Sci.*, 2011, **363**, 497-503.
  - W. Liu, M. Wang, C. Xu, S. Chen and X. Fu, *J. Mol. Catal. A Chem.*, 2013, **368**, 9-15.
  - H. Lee and W. Choi, *Environ. Sci. Technol.*, 2002, **36**, 3872-3878.